Appl Phys B (2009) 96: 545–560
DOI 10.1007/s00340-009-3582-0

Applied Physics B
Lasers and Optics

Self-adaptive, narrowband tuning of a pulsed optical parametric oscillator and a continuous-wave diode laser via phase-conjugate photorefractive cavity reflectors: verification by high-resolution spectroscopy

Y. He · B.J. Orr

Received: 2 March 2009 / Revised version: 6 May 2009 / Published online: 29 May 2009

Abstract A dynamic self-adaptive Bragg grating formed in a photorefractive crystal is shown to be a convenient way to attain single-longitudinal-mode (SLM) operation and narrowband tuning *both* in a pulsed, injection-seeded optical parametric oscillator (OPO) *and* in a continuous-wave (cw) extended-cavity diode laser. The pulsed OPO cavity comprises a Rh:$BaTiO_3$ photorefractive (PR) crystal, a periodically poled $KTiOPO_4$ nonlinear-optical crystal, and a dielectrically-coated end mirror. A continuous-wave seed beam at 820–850 nm from a tunable SLM diode laser traverses firstly the Rh:$BaTiO_3$ crystal and then is retro-reflected by the end mirror; this creates a wavelength-selective Bragg grating reflector in the PR crystal, thereby completing the OPO cavity. The cavity stays automatically resonant with the seed radiation, with no need to actively control its length or to make any other mechanical adjustment. One form of injection seeder comprises a novel extended-cavity diode laser (ECDL) design incorporating a self-pumped photorefractive phase-conjugate reflector and a compact, high-finesse tunable intracavity ring filter. This combination facilitates robust tunable single-frequency operation with narrow optical bandwidth. The performance characteristics of the OPO and the ECDL are evaluated by recording high-resolution atomic and molecular spectra. Notably, fluorescence-detected sub-Doppler two-photon excitation at 822 nm, of the $8S \leftarrow 6S$ transition in atomic Cs, provides a crucial linewidth test.

Y. He · B.J. Orr (✉)
MQ Photonics Research Centre,
Department of Physics and Engineering,
Macquarie University, Sydney, NSW 2109, Australia
e-mail: borr@physics.mq.edu.au
Fax: +61-2-98508115

PACS 42.65.Yj · 42.65.Hw · 42.55.Px · 42.60.Da · 42.62.Fi

1 Introduction

After a long history [1–4] of research on photorefractive (PR) effects, PR materials and applications based on PR devices, many significant issues and developments continue to be of current interest [5–7]. The central theme of this paper concerns the use of the popular crystalline PR material, rhodium-doped barium titanate (Rh:$BaTiO_3$) [8], as a medium in which dynamic, self-adaptive Bragg gratings can be generated to facilitate single-longitudinal-mode (SLM) operation and continuous narrowband tunability of two varieties of coherent near-infrared light source, namely:

(a) A pulsed, injection-seeded optical parametric oscillator (OPO) [9], and
(b) A continuous-wave (cw) extended-cavity diode laser [10]

Each of these devices (a) and (b) is intended for applications to high-resolution spectroscopy. This paper describes their innovative design details and operating characteristics, together with spectroscopic experiments to verify their performance.

Either approach (a) [9] or approach (b) [10] depends essentially on creating a dynamic intracavity reflector that is wavelength-selective and adaptable to wavelength changes. This is readily achieved via the PR effect, using a relatively low-power coherent light beam (typically in the mW range) albeit with relatively slow response time (typically seconds). Formation of a phase-conjugate reflector in a PR medium avoids the need for high optical power, as in other phase-conjugate reflection techniques that rely on instantaneous

nonlinear-optical interactions such as coherent four-wave mixing or stimulated Brillouin scattering.

Spatial and temporal effects associated with PR oscillators have been analyzed and demonstrated by Fischer et al. [11]. More recently, Pauliat et al. have elegantly reviewed self-organizing laser cavities [12], outlining how adjustment-free self-adaptive operation can be attained by means of an intracavity PR element. Various laser-related applications of photorefractivity, such as beam cleanup [13], have been implemented. Of particular interest in the present context, Omatsu et al. [14] have recently reviewed various ways in which PR phase-conjugate mirrors can be used to enhance the performance of solid-state optically pumped laser amplifiers and resonators and laser diodes. PR phase-conjugate feedback has been used in numerous forms of optically pumped solid-state laser [12, 14–19]. There are many more such instances of PR phase-conjugate feedback control of extended-cavity semiconductor diode lasers, both in narrowband single-stripe systems [10, 12, 14, 20–30] and in injection-locked broad-area or array devices [12, 31–43] with reduced optical bandwidth. Although dye lasers provided the earliest examples of PR phase-conjugate feedback as a way to control a laser's optical bandwidth [44, 45], there appear to have been no further reports in this context. Likewise, PR phase-conjugate feedback has been infrequently used as a means of controlling the optical bandwidth and tunability of output radiation from an OPO [9, 46–48].

In Sect. 2, we consider the role of PR phase-conjugate feedback in the design and performance of a pulsed, injection-seeded OPO, identified above as item (a) [9]. Section 3 gives details of a recently developed cw tunable diode laser with filtered PR phase-conjugate feedback, identified above as item (b), and explain the novelty of our approach [10] relative to the large body of prior literature in this area [12, 20–43]. Related spectroscopic measurements, devised to verify the performance of both items (a) and (b), are then described in Sect. 4.

2 Self-adaptive pulsed OPO with dynamic photorefractive grating

2.1 Pulsed OPO methodology

Pulsed OPOs have long been recognized [49–57] as potentially useful solid-state nonlinear-optical (NLO) sources of broadly tunable, coherent radiation for spectroscopic purposes, typically yielding high peak and average powers with pulse durations of ~10 ns. With advantages of high efficiency and wide tuning range (e.g., with respect to previously ubiquitous dye lasers), their early prospects [49–54] for laser spectroscopy have subsequently been realized in otherwise inaccessible spectral regions, such as the near- and mid-infrared [55–57]. It is often critical for such spectroscopic applications to finely control the OPO output wavelengths and their optical bandwidth. It is customary to tune the optical cavity of the OPO itself (e.g., by varying the cavity length or by incorporating a suitable intracavity wavelength-selective element) or by tuning the pump laser wavelength. Another efficient narrowband OPO tuning approach, extended within the last decade by our group [9, 54, 57–65] and others [66–73], is injection seeding by means of control radiation from an independent tunable low-power coherent light source.

In typical pulsed injection-seeded OPOs [57–73], continuous, mode-hop-free SLM tuning of signal and/or idler output requires active variation of the cavity length or some other form of mechanical adjustment and feedback stabilization (e.g., as in our well established "intensity dip" scheme [59–65]) as the wavelength λ_{seed} of the injection seeder is scanned. However, such active wavelength-control is not necessary in our *self-adaptive tunable* (*SAT*) *OPO* design [9], which we now describe in greater detail. The concept of this novel advance in injection-seeded OPO wavelength control is depicted schematically in Fig. 1. Identified as item (a) in Sect. 1, the SAT OPO employs a PR crystal (typically Rh:$BaTiO_3$) to serve as a phase-conjugate cavity mirror (M_1), in which a Bragg grating mirror is formed (typically within a few seconds) by photorefractive interaction between forward-propagating and retro-reflected cw seed beams. The reflectivity of this externally pumped PR phase-conjugate Bragg grating is centered at the wavelength λ_{seed} of the tunable cw seed laser and its wavelength-selectivity adapts automatically (without any mechanical adjustment of the OPO cavity) as λ_{seed} is scanned. The outcome of this pulsed injection-seeded SAT OPO design is a robust instrument that is simple to operate, offering continuous, self-adaptive SLM tunability and spectral narrowing of its signal and idler output radiation.

It should be recognized that the tunable cw laser radiation at wavelength λ_{seed} serves two simultaneous functions in facilitating operation of the SAT OPO, as follows:

(i) As explained above, it creates a phase-conjugate Bragg reflector in the PR crystal M_1, thereby automatically preparing the OPO cavity to be resonant at λ_{seed}.
(ii) As in any injection-seeded pulsed OPO, it pre-disposes the nonlinear-optical (NLO) medium $\chi^{(2)}$ to have a low oscillation threshold for the longitudinal mode of the OPO cavity that coincides with λ_{seed}, which is close to either λ_S or λ_I.

These distinct functions are inseparable in the SAT OPO and together account for the robust, adjustment-free SLM tunability and narrow optical bandwidth of its signal and idler output.

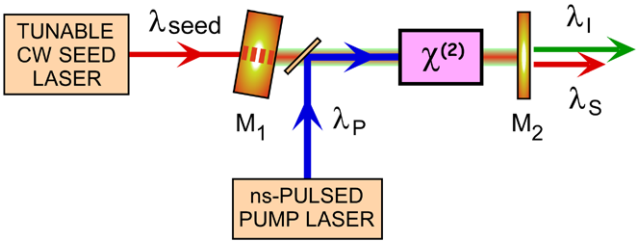

Fig. 1 Schematic diagram of a narrowband pulsed OPO, pumped by single-longitudinal-mode (SLM) coherent radiation at wavelength λ_P (e.g., 532 nm from a ns-pulsed, frequency-doubled Nd:YAG laser) with tunable signal and idler output beams at wavelengths λ_S and λ_I, respectively, controlled by injection seeding a suitable medium with nonlinear-optical susceptibility $\chi^{(2)}$ (e.g., periodically poled $KTiOPO_4$). The self-adaptive tunable (SAT) optical cavity includes a photorefractive (PR) crystal M_1 (e.g., Rh:$BaTiO_3$), in which a phase-conjugate Bragg grating is generated by interfering cw tunable seed laser light (at wavelength λ_{seed}) with its own back-reflection from cavity mirror M_2. The central wavelength of the induced reflective grating then tracks λ_{seed} as it is scanned, such that the injection-seeded OPO cavity stays resonant at λ_{seed} and is automatically controlled to yield continuously tunable SLM output at wavelengths λ_S and λ_I

2.2 Design and performance of the pulsed SAT OPO system

2.2.1 Implementation of the SAT OPO system

The SAT OPO approach has been realized with an OPO system based on periodically poled $KTiOPO_4$ (PPKTP) as the NLO medium, pumped at 532 nm by a frequency-doubled SLM Nd:YAG laser (Quanta-Ray GCR-250) with a pulse duration of ∼8 ns and a repetition rate of 10 Hz. The PPKTP crystal (Raicol Crystals; 1 mm × 2 mm × 20 mm, with a 9.35-μm grating period) is mounted in a temperature-controlled oven insulated with poly-(tetrafluoroethylene); this is settable to ±0.05°C, which enables coarse tuning of the OPO output wavelengths. The quasi-phase-matched tuning ranges for the signal and idler output from a corresponding free-running OPO are 818–875 nm and 1.52–1.36 μm, respectively, with PPKTP temperatures in the range 200–25°C [9, 64]. These free-running OPO signal and idler tuning ranges of ∼24 THz (∼800 cm^{-1}) are >3 times greater than that of any narrowband cw seed laser that is available to us. For instance, we have previously reported a seed-laser-limited continuous SLM tuning range of 7.5 THz (250 cm^{-1}) for an injection-seeded periodically poled $LiNbO_3$(PPLN) OPO with optoelectronic feedback control [61, 62].

The actual layout of our injection-seeded SAT OPO system (a) [9] is depicted schematically in Fig. 2 and a corresponding photograph of a OPO-cavity portion of the instrument is shown in Fig. 3. The linear OPO cavity is formed between the Rh:$BaTiO_3$ PR crystal, which serves as the phase-conjugate mirror M_1, and an end-reflector M_2 (plano-concave; 20-cm radius of curvature; anti-reflection coated for 532 nm; either 80% or ∼100% reflectivity at the 820–850-nm OPO signal wavelength). The cavity is ∼13 cm long, but could be shortened to achieve more amplification round-trips. The PPKTP crystal is tilted slightly to avoid interference by residual facet reflections. Figure 1 shows conceptually that the OPO idler output leaves the cavity through M_2. However, it is actually more convenient to extract the OPO signal output *either* as a 16% reflection off an uncoated surface of M_1 *or* via the exit port of the optical isolator. The only other intra-cavity component of the OPO is a pair of dichroic beam splitters BS (highly transmissive at wavelengths λ_S and λ_I and highly reflective at 532 nm); this is used to combine the pump- and seed-laser beams collinearly along the OPO cavity axis, each with linear polarization in the horizontal plane. The assembly of two dichroic beam splitters BS is used to ensure that no stray 532-nm pump radiation can propagate back to the PR crystal M_1, thereby avoiding possible damage.

In particular, it should be noted that the OPO cavity needs no provision for mechanical adjustment; once aligned, all cavity elements can remain rigidly in place as the output of the injection-seeded OPO is tuned by varying the wavelength of the external seed laser. In fact, as indicated in Fig. 3, the end-mirror M_2 is optionally mounted on a tubular piezoelectric translator (PZT; Physik Instrumente P-840.30) to allow minor variation of the cavity length and thus allow characterization of the PR phase-conjugate reflector M_1. The frequency stability of the SAT OPO is optimized by enclosing its cavity in a demountable box.

The pulse energy from the 532-nm pump laser is attenuated by means of a half-wave plate ($\lambda/2$) and thin-film polarizer (TFP) such that ∼100 μJ is incident on the PPKTP crystal. Various beam-conditioning lenses (L_1, L_2, etc.) are used to match the intra-cavity geometries of the pump- and seed-laser beams traversing the PPKTP crystal. Moreover, radiation from the seed laser is transmitted and spatially filtered by means of a 5-m single-mode optical fiber (cut-off wavelength <780 nm) via coupling lenses L_5 and L_6, before traversing an optical isolator (OFR IO-5-NIR-HP), comprising two linear polarizers and a 45° Faraday rotator.

The seed laser itself is a cw tunable diode laser, delivering SLM output with an optical power of several mW. Originally [9], we used *either* an external-cavity diode laser (New Focus 6316), that is widely tunable from 834 nm to 851 nm, *or* a distributed-feedback diode laser (SDL 5702-H1) with limited tunability by temperature at ∼851.5 nm. More recently, we have employed our newly developed form of cw extended-cavity diode laser system [10]; this is tunable from ∼820 to ∼840 nm and has been identified as item (b) in Sect. 1. As will be demonstrated in Sects. 3 and 4 below, its optical frequency stability is superior to that of the two commercially available cw tunable diode lasers that we had previously used [9].

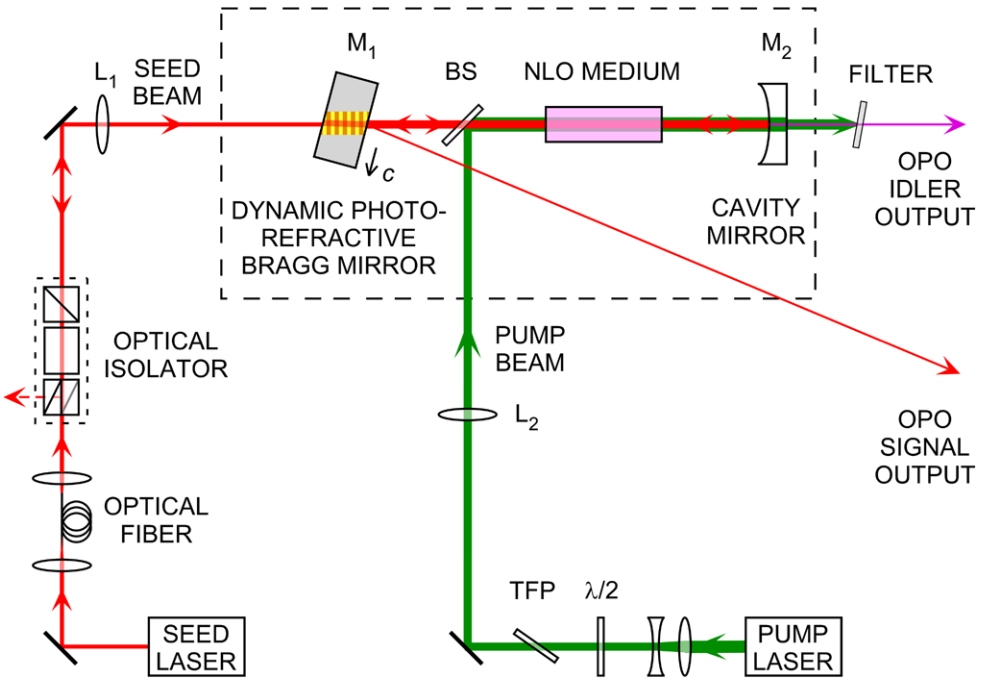

Fig. 2 Layout of a narrowband ns-pulsed PPKTP SAT OPO, pumped at 532 nm by a frequency-doubled Nd:YAG laser and tuned by injection seeding via a self-adaptive phase-conjugate cavity mirror M_1 based on a Rh:$BaTiO_3$ PR crystal. The *dashed lines* depict a demountable enclosure to optimize frequency stability of the OPO. See text for further details

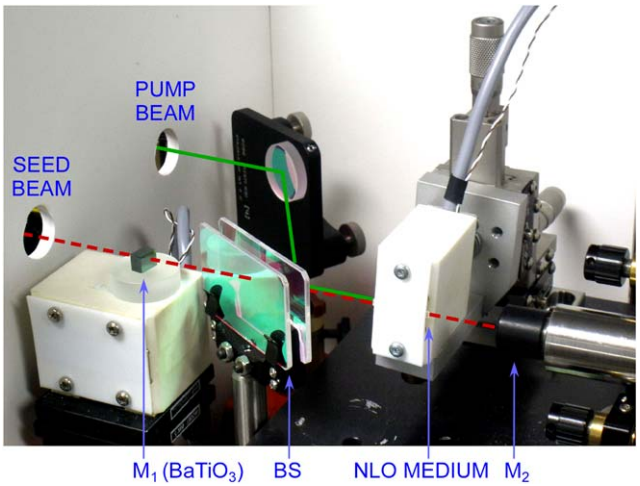

Fig. 3 Photograph of the OPO-cavity portion of the SAT OPO system (as depicted schematically, enclosed by a *broken line*, in Fig. 2). Optical components shown (*left* to *right*) are: Rh:$BaTiO_3$ PR photorefractive cavity mirror M_1; dichroic beam splitter BS; PPKKTP NLO crystal in its temperature-controlled mount; end-mirror M_2 (on an optional tubular PZT mount). The OPO cavity axis (and seed-beam path) is denoted by a *dashed line* and the pump-beam path by an *unbroken line*. See text for further information

The Rh:$BaTiO_3$ PR crystal (Dynoptic Components; 7.5 × 5 × 5 mm along the crystal axes c, a, and a, respectively) is a key optical control element (M_1) in the SAT OPO; its specified actual Rh dopant concentration is ∼6 p.p.m. (corresponding to 600 p.p.m. Rh in the initial mixture used to prepare the crystal) and each of its six facets is optically polished but uncoated (yielding ∼16% loss per surface). The Rh:$BaTiO_3$ crystal is mounted with one of its two a-axes vertical (perpendicular to the horizontal plane of polarization of the pump and seed radiation); the horizontal c-axis is aligned ∼80° away from the OPO-cavity axis (as indicated in Fig. 2), to avoid interfering reflections by crystal surfaces and to provide a convenient way to couple signal output radiation out of the OPO cavity.

As already outlined in Fig. 1 and Sect. 2.1 above, the cw seed-laser beam enters the OPO cavity through the Rh:$BaTiO_3$ crystal, traverses its PPKTP NLO crystal, and is retro-reflected by mirror M_2. Fine adjustment of lenses L_4 and L_6 enables the geometry of the seed beam retro-reflected by mirror M_2 to be matched to that of the incoming seed beam. The two counter-propagating cw seed beams then interfere most efficiently within the Rh:$BaTiO_3$ PR crystal, so that a phase-conjugate Bragg grating is formed within a few seconds. Once the PR grating is formed, the Rh:$BaTiO_3$ crystal M_1 becomes partially reflecting for a narrow band of wavelengths centered at the seed wavelength λ_{seed} used to generate the grating. With an incident seed-laser power of several mW, the maximum attainable reflectivity of M_1 was measured to be approximately 60%. Moreover, the PR grating adapts itself to changes of seed wavelength λ_{seed}, so that the SAT OPO cavity remains resonant at λ_{seed} as the seed laser is gradually tuned. We report further performance characteristics of this externally pumped PR phase-conjugate Bragg reflector M_1 in Sect. 2.2.2 and of the overall OPO system in Sect. 2.2.3.

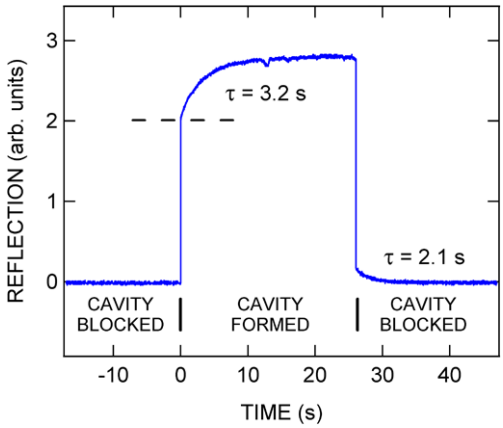

Fig. 4 Back reflection of the seed beam (1.7 mW cw at ∼850 nm from the SDL DFB diode laser) by the Rh:$BaTiO_3$ PR crystal from an empty cavity (with the PPKTP NLO crystal and the dichroic beamsplitter M_3 removed) that is successively blocked and unblocked. The time constants τ are obtained from exponential fits. See text for further explanation

2.2.2 *Temporal and bandwidth characteristics of the PR phase-conjugate grating*

The temporal characteristics of the Rh:$BaTiO_3$ PR phase-conjugate reflector M_1 are demonstrated in Fig. 4. These measurements were made with an empty cavity (i.e., the PPKTP NLO crystal and the dichroic beamsplitter assembly BS have been removed from the SAT OPO cavity) and by monitoring the retro-reflected seed beam that is diverted by the optical isolator, as shown in Fig. 2. This empty cavity was then blocked and unblocked rapidly by an internal shutter located between M_1 and M_2, to successively write and erase the PR phase-conjugate Bragg grating every 25–30 s. Figure 4 shows an instantaneous increase/decrease in reflected power when the cavity is unblocked/blocked, followed by exponential growth/decay, with time constants τ of 3.2 s (growth) and 2.1 s (decay) when the cw seed-beam power incident on the Rh:$BaTiO_3$ crystal M_1 is 1.7 mW. These time constants τ decrease as the seed-beam power is increased; the differences between τ for growth and decay might be associated with ∼16% reflection losses at each crystal surface and minor absorption losses in the bulk crystal. If the Rh:$BaTiO_3$ PR crystal is not exposed to an erasing seed beam, then the PR phase-conjugate Bragg grating decays with a relatively long time constant (exceeding 70 s), which is independent of the total dose of seed radiation that had been used to create the PR phase-conjugate Bragg grating.

As mentioned in Sect. 2.2.1 above, the end-mirror M_2 is optionally mounted on a PZT, which allows the cavity length to be varied piezoelectrically. This has enabled us to perform experiments that characterize the operation of the fully assembled SAT OPO (i.e., with the PPKTP NLO crystal returned to the cavity and pumped at 532 nm via the dichroic beam splitter BS, as shown in Figs. 2 and 3) with the retro-reflected cw seed beam generating a Bragg grating in the PR Rh:$BaTiO_3$ crystal M_1, with constant λ_{seed}. In one experiment, the PZT was used to introduce successive abrupt steps in the cavity length of the SAT OPO, causing the idler output power to vary as the Bragg grating is re-written at each PZT-voltage step and the SAT OPO output adapts to a different cavity length. Likewise, stepping the unpumped cavity length resulted in an instantaneous decrease in back-reflection from the PR Rh:$BaTiO_3$ crystal M_1 (as in the context of Fig. 4) followed by gradual recovery of reflectivity. Each of these PZT-induced responses occurs on a time-scale similar to that in Fig. 4.

In our preliminary paper [9], we reported a "write-and-probe" experiment to measure the wavelength selectivity of the phase-conjugate mirror M_1. Initially, the Bragg grating was formed by using the 1.7-mW cw SLM seed beam from a distributed-feedback (DFB) diode laser to irradiate the PR Rh:$BaTiO_3$ crystal at an arbitrarily fixed wavelength ∼850 nm. The seed beam was then abruptly blocked to enable the reflectivity spectrum of M_1 to be probed before there was significant decay of the Bragg grating that had been created (i.e., within less than 10% of the persistence time τ of ∼70 s in the dark). This was performed by means of a very weak probe beam (less than 25 μW) from a second SLM DFB diode laser, also operating at ∼850 nm. The optical frequency of the probe laser was tuned in a 5-s scan over a range of ∼90 GHz centered on the frequency of the SLM seed light that had been used to induce the PR grating. The resulting reflectivity spectrum [9] displayed a bandwidth of 14 GHz (∼0.5 cm^{-1}) FWHM, which is consistent with expectations [74] for a "weak" Bragg grating, in which the reflectivity bandwidth is inversely proportional to the path-length through the PR crystal.

2.2.3 *Conversion efficiency and tuning characteristics of the pulsed SAT OPO*

As shown in Fig. 5, the power-conversion operating characteristics for the fully assembled SAT OPO system seeded at ∼850 nm have been measured by means of a power meter (Ophir PE10-SH). The vertical error bars show the upper and lower bounds of numerous repeated measurements, with a typical uncertainty of ±0.2 μJ. The oscillation threshold is found to be at a 532-nm pump-laser pulse energy of ∼40 μJ. The maximum idler output pulse energy at ∼1.42-μm transmitted by end-mirror M_2 is measured to be 6.4 μJ (allowing for 16% reflection loss due to four uncoated glass surfaces); this is generated with a 532-nm pump-laser pulse energy of 94 μJ incident on the PPKTP NLO crystal (∼2.3 times above threshold), which corresponds to a slope efficiency of ∼12%. The overall slope efficiency for conversion of the combined signal and idler radiation is estimated to be

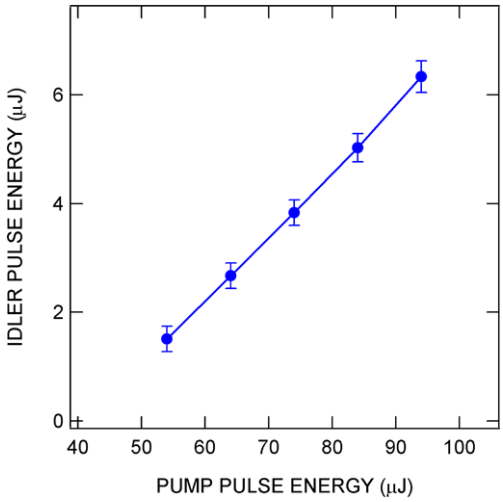

Fig. 5 Power-conversion operating characteristics for the SAT OPO, with pulse energies of idler output at ∼1.42-μm plotted as a function of pump-laser pulse energy. *Error bars* show upper and lower limits of measurements

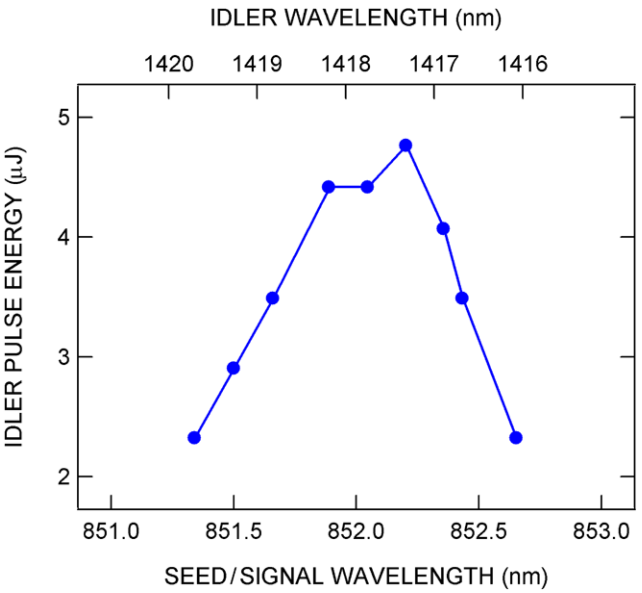

Fig. 6 Idler output pulse energy plotted as a function of seed wavelengths within the gain bandwidth of the SAT OPO at a constant PPKTP crystal temperature of 98°C

∼33%. The pump laser has reserve power available to drive one or more amplifier stages for higher-power applications, if necessary.

The continuous tuning range of the SAT OPO, with the temperature of its PPKTP NLO crystal fixed at 98°C, is demonstrated in Fig. 6. With a 532-nm pump-laser pulse energy of ∼80 μJ, idler pulse energies (in the range of 1.420–1.416 μm) are plotted versus the injection-seeded wavelength (coinciding necessarily with the signal output wavelength, ranging from ∼851.3 to ∼852.7 nm). The resulting OPO conversion curve is consistent with the well-established NLO characteristics of PPKTP [75, 76].

By measuring interferometer interference fringes (e.g., using a Burleigh WA-4500 pulsed wavemeter), we have verified that the SAT OPO output can be scanned continuously without mode hops within such a fixed-temperature tuning range. Such measurements indicate that the instrument is capable of reliable SLM operation, with optical bandwidth close to the Fourier-transform limit, as the wavelength of the cw injection seeder is slowly scanned. This mode-hop-free continuous tunability is further (and even more convincingly) confirmed by direct spectroscopic measurements that are presented in Sect. 4 below.

Even without the narrowband SLM tunability that is afforded by injection-seeded operation (identified as contributing process (ii) in Sect. 2.1), the wavelength selectivity of the phase-conjugate mirror M_1, as measured [9] in our write-and-probe experiment (see Sect. 2.2.2 above), is significant. The measured 14-GHz FWHM reflectivity bandwidth of M_1 [9] is a factor of ∼10 less than the optical bandwidth of a corresponding free-running PPKTP OPO, namely, ∼150 GHz (∼5 cm^{-1}). The implication is that formation of a phase-conjugate mirror M_1 in the PR Rh:$BaTiO_3$ crystal (identified as contributing process (i) in Sect. 2.1) can by itself result in substantial spectral narrowing of OPO output radiation.

3 Cw extended-cavity diode laser (ECDL) with filtered PR phase-conjugate feedback

3.1 Cw ECDL methodology

In Sect. 2, we have considered the role of PR phase-conjugate feedback in the design and performance of a pulsed, injection-seeded OPO, identified in Sect. 1 as item (a) [9]. Here, in Sect. 3, we now address details of a recently developed cw tunable diode laser with filtered PR phase-conjugate feedback, identified in Sect. 1 as item (b) [10].

Fabry–Perot semiconductor lasers are well established as convenient coherent light sources. However, their short cavity length (typically <1 mm) allows small changes in drive current, junction temperature, or optical feedback to result in longitudinal-mode instability, mode hopping, and spectral broadening. It is therefore customary to enhance optical bandwidth and frequency stability by incorporating a bare laser diode in an extended cavity. This approach enables laser frequency to be actively controlled and stabilized by fast discrimination of frequency changes, combined with optoelectronic feedback to frequency-control components [77]. Narrow optical bandwidth can also be achieved by simpler passive forms of wavelength-selective optical feedback [78, 79], in which the laser frequency is locked to a rigid,

low-drift external cavity. However, the laser wavelength is then usually not well defined and is inclined to hop among numerous resonant modes of the feedback cavity within the gain envelope of the laser. There are many forms of external- or extended-cavity diode laser (ECDL), with their output wavelength and linewidth controlled in assorted ways (e.g., by an intracavity diffraction grating, either Littrow-mounted or grazing-incidence) [80–89].

Phase-conjugate feedback from a PR crystal has long been recognized [21] as a way to reduce laser linewidth. As already indicated in Sect. 1, this approach has already been used to control numerous forms of *extended-cavity diode laser* (*ECDL*): both single-stripe ECDLs [10, 12, 14, 20–30] and injection-locked broad-area or array ECDLs [12, 31–43]. Laser operation can vary from chaotic to SLM, depending on the strength of optical feedback (e.g., feedback above ∼22% yields SLM operation) [25, 38]. Although phase-conjugate optical feedback is able to induce SLM laser operation, the laser frequency is prone to self-induced scanning [20, 29, 34–36, 44, 45], so that such feedback will not necessarily ensure stable tunability of the ECDL unless special measures are taken to reduce self-induced scanning [30, 34–36].

Our novel form of narrowband-tunable ECDL [10] is based on a combination of *self-pumped phase-conjugate* (*SPPC*) *feedback* from a PR crystal and *intracavity SLM filtering*. A particular longitudinal mode of the ECDL cavity is defined by means of a high-finesse intracavity filter and further enhanced by the wavelength-adaptive narrowband reflectivity of the SPPC feedback. This ensures robust, well-controlled narrowband (i.e., SLM) tunability of the ECDL without mode hops when the output wavelength needs to be continuously scanned.

It should be noted that the present *self-pumped PR* (SPPC) approach to feedback control in the case of our ECDL (b) [10] is distinct from the *externally pumped PR* approach employed in the case of our SAT OPO (a) [9], which relies on an independently tunable narrowband seed laser (as explained in Sect. 2 above). In the externally pumped PR OPO case (a), limitations imposed by the 14-GHz FWHM wavelength-selective reflection bandwidth of the PR Bragg grating itself [9] are overcome by the fact that the tunable cw laser radiation performs an injection-seeding function (ii) as well as generating the phase-conjugate Bragg grating in the Rh:$BaTiO_3$ PR crystal M_1 (i). In the self-pumped PR (SPPC) case of our ECDL (b), a reflection bandwidth of 12 GHz has been reported for a similar ECDL system containing a SPPC reflector based on a Cr:$BaTiO_3$ PR crystal [90]. To constrain and define the laser wavelength, the intracavity filter therefore needs to have a free spectral range larger than the reflection bandwidth of the PR Bragg grating, so that only one mode of the filter's transmission spectrum falls within that bandwidth. To ensure that only one longitudinal mode is favored at any time, the filter must have a high finesse, so that its transmission bandwidth matches the longitudinal-mode spacing of the SPPC ECDL cavity. Design criteria of this type have been implemented in the SPPPC ECDL design described in detail in Sect. 3.2 below.

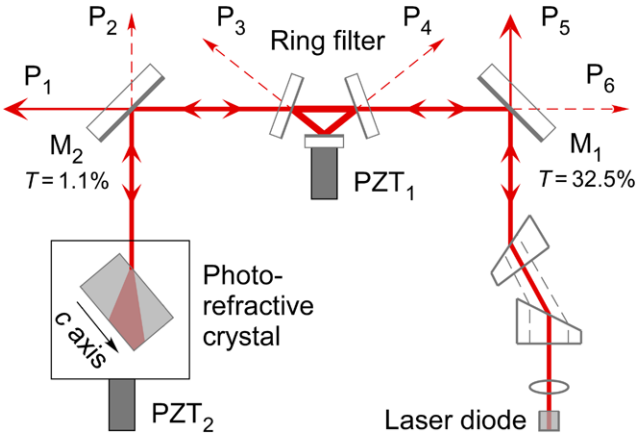

Fig. 7 Layout of an external-cavity diode laser (ECDL) system, with an optical feedback scheme for frequency stabilization and tuning based on a combination of wavelength-selective self-pumped phase-conjugate (SPPC) reflection by a photorefractive crystal and of intracavity single-longitudinal-mode (SLM) filtering

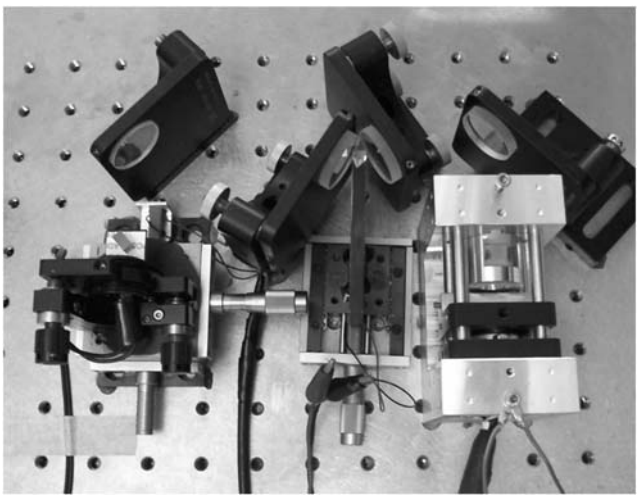

Fig. 8 Photograph of the SPPC ECDL system, paralleling the layout shown in Fig. 7. The laser diode mount (with cover removed to reveal its beam-shaping optics) is in the lower right-hand portion of the photograph, the compact 3-mirror ring-cavity filter (with its relatively bulky micro-positioning control mechanism) is central, and the photorefractive crystal (also micro-positioned) is on the *left*. The scale is indicated by the 25-mm spacing of tapped holes on the optical breadboard

3.2 Design and performance of the cw SPPC ECDL

3.2.1 Implementation of the cw SPPC ECDL system

The basic layout of our cw ECDL system [10] is illustrated in Fig. 7, together with a corresponding photograph

in Fig. 8. It comprises a simple Fabry–Perot laser diode, together with a miniature high-finesse 3-mirror ring filter and a Rh:$BaTiO_3$ PR crystal which serves as the SPPC feedback element. The extended laser cavity is formed between the back facet of the laser diode and the PR crystal, which builds up SPPC feedback. The main beam paths are traced as solid lines in Fig. 7. Laser radiation is accessible at various positions via partially transmissive mirrors (M_1 and M_2). Two piezoelectric micropositioners (PZT_1 and PZT_2; Thorlabs AE0505D18) are used to control the optical path lengths of the laser cavity and the 3-mirror ring filter, respectively.

We have used a Fabry–Perot index-guided laser diode (JDS Uniphase SDL-5412-H1) operating in the wavelength range of 820–840 nm, with an integrated thermoelectric Peltier element for temperature control. The output frequency of the bare diode laser depends sensitively on both diode current and temperature, with coefficients of 1.6 GHz mA^{-1} (0.053 $cm^{-1}\,mA^{-1}$) and 22.8 GHz $°C^{-1}$ (0.76 $cm^{-1}\,°C^{-1}$), respectively. We have monitored the wavelength and mode structure of the laser output by means of a scanning Fabry–Perot spectrum analyzer (TecOptics) and a wavemeter (Burleigh WA-4500) with a resolution of ∼0.1 pm (∼0.04 GHz; 0.0013 cm^{-1}). In the absence of an external cavity, it is found that SLM operation of the bare Fabry–Perot laser diode can occur under certain conditions. However, the resulting spectral linewidth is estimated to exceed 100 MHz, so that such a bare Fabry–Perot laser diode would not by itself be amenable to high-resolution spectroscopic applications. In a typical Fabry–Perot index-guided laser diode, spectral broadening, mode hopping, mode pulling, and longitudinal-mode instability may arise owing to tiny changes in drive current, diode junction temperature or optical feedback with reflected fractional power levels as low as 10^{-8} [91].

The beam of radiation from the laser diode is collimated by an aspherical lens and then shaped into a circular cross section by a pair of anamorphic prisms. Useful beams of output laser radiation emerge through the mirrors M_1 and M_2, which have partial transmissions of 32.5% and 1.1%, respectively. The ECDL cavity is enclosed in a box to optimize frequency stability by minimizing atmospheric and thermal fluctuations.

The Rh:$BaTiO_3$ PR crystal (Dynoptic Components; 8.2 × 6.6 × 5.1 mm along the crystal axes c, a, and a, respectively) has a specified actual Rh dopant concentration of ∼6 p.p.m.; each of its six facets is optically polished but uncoated (yielding ∼16% loss per surface). It is mounted with its shorter a-axis vertical (perpendicular to the horizontal plane of polarization of the laser radiation); the horizontal c-axis is carefully aligned to allow the SPPC reflection to build up with its characteristic optical "fan-out" pattern from a corner of the crystal (typically with an angle of beam incidence of ∼55°, as indicated in Fig. 7). Changes in temperature of the PR crystal (which is maintained at ∼40°C) effectively alter the cavity length, as does variation of the voltage applied to PZT_1.

The compact, high-finesse intracavity ring filter is a vital element of the SPPC ECDL system, providing the necessary additional frequency selectivity for continuously tunable SLM laser operation. It comprises three plane mirrors (two partial reflectors and one high reflector) arranged in the form of an isosceles triangle; its resonance frequencies can be finely tuned by means of PZT_2 at the symmetric apex of the triangle. The path length of the ring filter is 1.5 cm, which corresponds to a mode spacing of 20 GHz (0.67 cm^{-1}). The optical transmission loss of the ring filter is slightly less than 20%; ideally, this could be reduced much closer to zero by coating the PZT_2-controlled apical mirror for 100% reflectivity. Other observed performance characteristics are reported in Sect. 3.2.2 below.

To initiate operation of the SPPC ECDL system, the frequencies of the free-running diode-laser and of the ring filter are brought into coincidence, so that laser radiation can traverse the ring filter to reach the PR crystal. This is done by varying the diode temperature and/or the voltage applied to PZT_2 (for the diode laser and ring filter, respectively). The self-pumped Bragg grating then builds up in the Rh:$BaTiO_3$ PR crystal within less than ∼10 minutes, attaining a reflectivity that we measure to be as high as ∼66% (by comparing optical powers transmitted by M_2 on paths P_2 and P_1 and allowing for the partial reflectivity of M_2).

Once formed, the self-pumped PR grating adjusts to wavelength changes within a few seconds. In the absence of light, the grating typically persists for ∼1 hour; this long decay time conveniently enables the operating frequency of the laser to be resumed after short interruptions. In the start-up period, when the SPPC reflection is building up and the level of optical feedback is low, the laser is found to oscillate on several (typically ∼5) modes of the ring filter. Stable SLM operation is established once the strength of feedback to the laser diode reaches ∼3%. This level of feedback from the extended cavity (comprising ring filter and PR crystal) to the laser diode has been determined by comparing optical powers transmitted by M_1 on paths P_6 and P_5 (with allowance for the partial reflectivity of M_1).

3.2.2 *Tuning characteristics of the cw SPPC ECDL system*

The intracavity 3-mirror ring filter has been further characterized by measuring its reflection of free-running cw diode laser radiation. To achieve this, we run the laser at a single fixed frequency (with SPPC feedback from the PR crystal blocked) and use PZT_2 to scan the filter cavity rapidly over ∼2 free spectral ranges while monitoring the optical power reflected along path P_4. The outcome, plotted in Fig. 9, yields a finesse of ∼30, which indicates that the overall intracavity reflectivity of the 3-mirror ring filter is ∼90%.

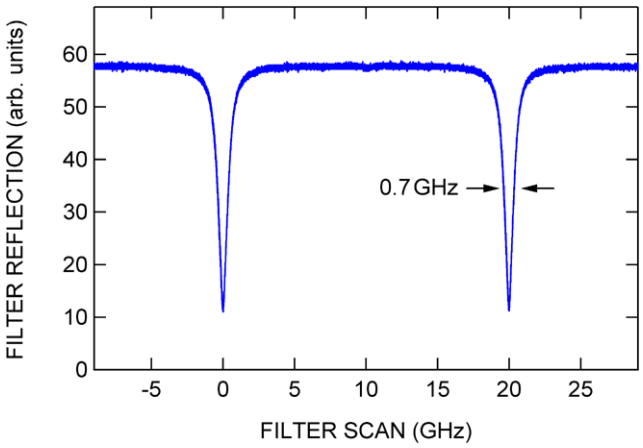

Fig. 9 Reflection of free-running cw diode laser radiation at ∼822.5 nm off the compact 3-mirror ring-cavity filter, the round-trip length of which is scanned over a distance of ∼1.6 μm within a 70-ms period. The optical path length of the ring cavity is ∼1.5 cm, resulting in a free-spectral-range mode spacing of ∼20 GHz. This compact ring cavity, with a finesse of ∼30, acts as an optical filter with a FWHM width of ∼0.7 GHz

The corresponding half-width-at-half-maximum transmission width of ∼0.33 GHz (∼0.011 cm^{-1}) is sufficiently narrow to be compatible with the ∼0.48-GHz (∼0.016-cm^{-1}) mode-spacing of the 31-cm extended laser cavity and to facilitate SLM tunability.

We have previously reported how the laser output wavelength depends on the tuning of the ring filter by an analog ramp voltage applied to PZT_2 (see that Fig. 2 of our preliminary report [10], not reproduced in this paper). The laser wavelength is found to scan smoothly for small changes, typically ∼1 pm (∼0.4 GHz; 0.013 cm^{-1}), of the ring-filter resonance before it hops forward to the next longitudinal mode of the extended laser cavity as that particular mode approaches the filter resonance. Such results [10] have confirmed that, as intended, the laser operates on a longitudinal mode that is defined by the ring filter.

Further verification of the single-frequency tunability of the SPPC ECDL system is obtained by fixing the resonance frequency of the ring filter and shifting the PR crystal to scan the length of the extended laser cavity by means of PZT_1. As previously presented in Fig. 3 of our preliminary report [10], Fig. 10(a) of this paper shows that the laser wavelength (upper curve) resides on the longitudinal cavity mode which is closest to the ring-filter resonance and scans smoothly over a range of ∼0.6 pm (∼0.24 GHz; 0.008 cm^{-1}) for a small change of extended cavity length, as determined by the PZT_1 sawtooth ramp voltage (lower trace). The smaller 0.1-pm steps in the laser wavelength plots are attributable to the limited resolution of the wavemeter. Beyond the short SLM tuning range of ∼0.6 pm, the laser wavelength is seen to hop back by ∼0.7 pm when the next longitudinal mode of the extended laser cavity is closer to the filter resonance. Figure 10(b) shows simultaneous measurements of

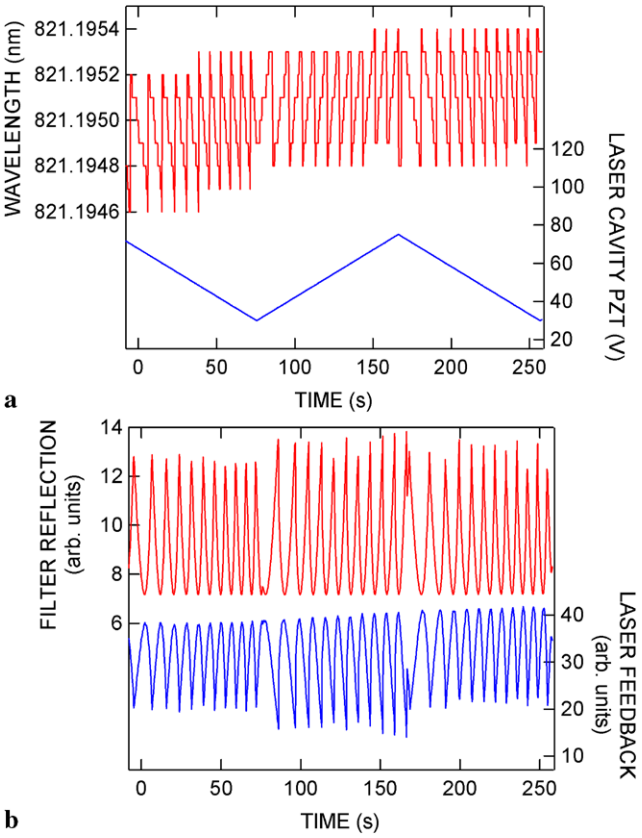

Fig. 10 Demonstrations of single-frequency tunability of the SPPC ECDL system, simultaneously measured as the length of the extended laser cavity is piezoelectrically scanned, with the resonance frequency of the 3-mirror ring-cavity filter fixed. (**a**) The dependence of laser output wavelength (*upper trace*) as the length of the extended laser cavity is varied by means of the voltage applied to PZT_1 (*lower trace*) [10]; the laser wavelength scans smoothly around the resonance of the ring-cavity filter for small changes of cavity length, then hops back to the next mode of the laser cavity as it approaches the filter resonance; the small steps of 0.1 pm in wavelength reading are due to wavemeter resolution. (**b**) Concurrent measurements (via optical paths P_4 and P_6 in Fig. 7) of laser light reflected from the 3-mirror ring-cavity filter (*upper trace*) and SPPC light fed back to the laser cavity (*lower trace*); precise resonance with the filter occurs at each reflection minimum and each feedback maximum

the laser light reflected from the ring filter (upper trace) and the SPPC light that is fed back to the laser cavity (lower trace); these are measured respectively via optical paths P_4 and P_2 (dashed arrows in Fig. 7). Precise resonance with the ring-cavity filter occurs at each minimum/maximum in the upper/lower trace of Fig. 10(b). Incidentally, successive sawtooth scans show a small drift in wavelength readings (typically ∼0.22 pm during a 180-s full-wave PZT_1 ramp cycle) that is attributable to PZT and wavemeter drift effects; this is ∼3 times less than in the previous case [10] where the ring filter was scanned and the extended laser cavity fixed.

In further experiments, we have simultaneously scanned both the ring-filter resonance and the length of the extended laser cavity, as demonstrated by Fig. 11, to realize more ex-

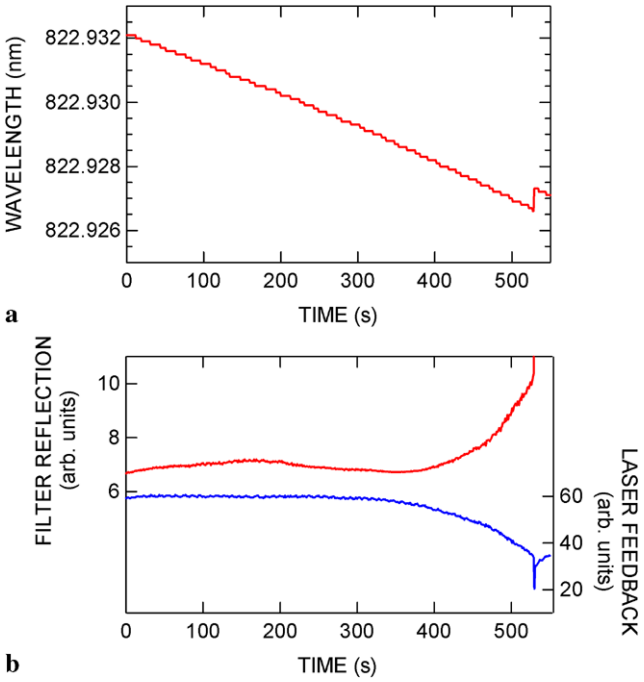

Fig. 11 Evidence of extensive mode-hop-free tuning of the SPPC ECDL system, achieved during a continuous scan of laser wavelength by simultaneously tuning the lengths of both the laser cavity and of the 3-mirror ring-cavity filter. (**a**) Wavemeter measurements of the laser wavelength, spanning ∼5.5 pm during a 9-minute scan; the small steps in the wavelength plot are due to the digital resolution of 0.0001 nm (∼44.3 MHz) of the wavemeter. (**b**) Plots of filter reflection (*upper trace*) and SPPC feedback (*lower trace*), measured concurrently as in Fig. 10(b). Towards the end of each scan in (**a**) and (**b**), a mode hop occurs; this abrupt event in (**a**) is preceded ∼2 minutes beforehand by upward and downward excursions in (**b**) of the filter reflection and SPPC feedback, respectively

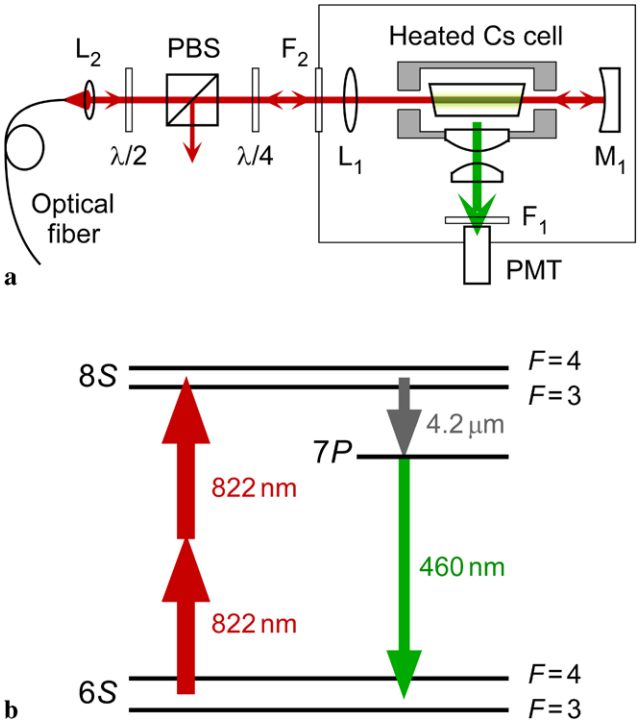

Fig. 12 Sub-Doppler two-photon excitation (TPE) spectroscopy of atomic Cs. (**a**) Experimental setup, in which a single-mode optical fiber delivers tunable coherent radiation at ∼822.5 nm from *either* a cw diode laser *or* a pulsed OPO; sub-Doppler TPE by counter-propagating laser beams is detected by spontaneous fluorescence. (**b**) $8S \leftarrow 6S$ TPE of Cs has two hyperfine components, each with $\Delta F = 0$, at 822.4595 nm ($F = 3$) and 822.4689 nm ($F = 4$), detected by cascaded $7P \rightarrow 6S$ fluorescence at ∼460 nm. See text for details

tensive mode-hop-free tuning. Figure 11(a) shows a continuous SLM laser frequency scan spanning more than 5 pm (∼2 GHz; ∼0.07 cm^{-1}), accompanied in Fig. 11(b) by corresponding simultaneous measurements of ring-filter reflection (upper trace) and SPPC feedback (lower trace), as in Fig. 10(b). Towards the end of this scan, the drift of the laser cavity and of the filter are seen to lose synchronization as the upper/lower trace departs from its on-resonance minimum/maximum, finally resulting in a mode hop after an elapsed time of ∼540 s (9 minutes). The ability to sustain mode-hop-free SLM scans of the laser frequency for a relatively long period of time shows that the cw SPPS ECDL has much potential for high-resolution spectroscopy and also for stable, narrowband injection-seeded operation of pulsed OPO systems (e.g., the SAT OPO discussed in Sect. 2).

4 Spectroscopic measurements

We have made assorted spectroscopic measurements to test the performance of both the pulsed SAT OPO system and the cw SPPC ECDL system. These experiments comprise sub-Doppler two-photon excitation spectroscopy, as reported in Sect. 4.1, and linear cavity-ringdown absorption spectroscopy, as reported in Sect. 4.2.

4.1 Sub-Doppler two-photon spectroscopy in Cs

4.1.1 Detection of the $8S \leftarrow 6S$ two-photon transition in Cs

Sub-Doppler *two-photon excitation* (*TPE*) *spectroscopy* has been used on numerous occasions to demonstrate the narrowband tunability of signal or idler radiation from various forms of pulsed injection-seeded OPO, detected *either* by ionization in a Ba atomic beam [92] *or* by laser-induced fluorescence (LIF) in Rb [93, 94], NO [95] and Cs [96, 97] vapor.

Of particular relevance here is the LIF-detected sub-Doppler TPE spectrum of the $8S \leftarrow 6S$ transitions in atomic cesium (Cs) at ∼822.5 nm, which has provided a crucial optical-bandwidth test for a high-performance long-pulse PPKTP OPO system [96, 97] and also the cw SPPC ECDL system described in Sect. 3 [10]. The layout of our TPE LIF spectrometer, with counter-propagating

OPO or laser beams and orthogonal LIF detection, is illustrated in Fig. 12(a), together with the associated spectroscopic excitation scheme Fig. 12(b). Cs atoms have two $8s^2S_{1/2} \leftarrow 6s^2S_{1/2}$ two-photon hyperfine transitions, each with $\Delta F = 0$: at 822.4595 nm ($F = 3$) and at 822.4689 nm ($F = 4$) [98–100]. Each of these two TPE features has a natural linewidth of ∼1 MHz and can be detected by means of cascaded $7P \rightarrow 6S$ fluorescence at ∼460 nm, as depicted schematically in Fig. 12(b) [98–101]. We note that similar excitation and detection schemes have been used recently to stabilize the frequency of 822.5-nm lasers [102, 103] and to refer spectroscopic transitions of atomic Cs to those of highly accurate frequency combs [100, 103].

As depicted in Fig. 12(a), the TPE LIF spectrometer comprises a cylindrical fused-silica cell (15 mm dia. × 75 mm long; Triad Technology, TT-CS-75-V-Q) with wedged windows mounted at an angle to the cell axis to reduce unwanted back-reflection. This cell contains a bead of metallic Cs and is mounted inside a stainless-steel block that is resistively heated (typically at ∼90°C, yielding a Cs vapor pressure of ∼0.1 mTorr), with heating elements located close to the cell windows, and thermally insulated. Coherent 822-nm radiation, from *either* the cw SPPC ECDL *or* the signal wave of the pulsed SAT OPO, traverses a long-pass filter F_2 (Schott RG715, with 715-nm cut-on wavelength), this radiation is focused by a spherical lens L_1 (focal length = 20 cm) into the center of the Cs vapor cell. A concave mirror M_1 (radius of curvature = 20 cm) at the other end of the cell reflects the beam back to establish the counter-propagating geometry and precise spatial overlap necessary for efficient sub-Doppler TPE. The incident 822-nm laser light is delivered via an optical isolator (OFR IO-5-NIR-HP); not shown in Fig. 12(a) and a single-mode optical fiber (Thorlabs FS-SH-4224) and collimating lens L_2. Alignment of the returning beam is optimized by fine adjustment and monitoring its coupling back through the single-mode fiber. A half-wave plate ($\lambda/2$), polarizing beam splitter (PBS), and quarter-wave plate ($\lambda/4$) are also available to provide optional TPE by circularly polarized light; in *S*–*S* TPE spectra, this suppresses Doppler pedestals which can be excited by co-propagating linearly polarized light.

The inside wall of the stainless-steel sample-cell block is finely machined to act as a reflector that effectively doubles the collection efficiency for the 460-nm fluorescence. This fluorescence is monitored through a rectangular (20 × 50 mm) side opening in the block via a suitable combination of a cylindrical lens (focal length 25.4 mm, dimension 25.4 × 51 mm) and a spherical plano-convex lens (focal length 60 mm, diameter 51 mm) by a photomultiplier tube (PMT; Hamamatsu 1P-28) and fast preamplifier (Stanford Research Systems SR445) with a combined rise-time of ∼2.5 ns. Unwanted scattered and background light are minimized by placing a bandpass filter F_1 (Schott BG40) in front of the PMT and by enclosing the Cs cell assembly in an opaque box. The body of the PMT itself is located outside the light-shielding box to avoid the high temperature of the heated Cs cell.

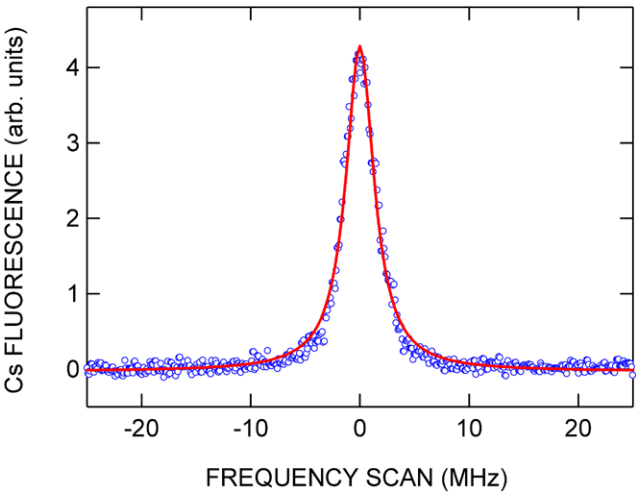

Fig. 13 Sub-Doppler TPE spectrum of the $8s\ ^2S_{1/2} \leftarrow 6s\ ^2S_{1/2}$, $F = 4$ hyperfine transition of Cs, recorded (○) by frequency-scanning the SPPC ECDL at ∼822.4689 nm and photon-counted fluorescence detection. The Lorentzian-profile fit (*solid trace*) has a 3.1-MHz FWHM

When working with cw SPPC ECDL radiation, the 460-nm fluorescence collected by the PMT is processed by a photon counter (Stanford Research Systems SR400). In the other cases, fluorescence signal arising from TPE by pulsed SAT OPO radiation is PMT-detected in analog mode, sampled by a fast digital oscilloscope (Tektronix TDS3054, 500-MHz bandwidth), and integrated by computer, typically for ∼400 ns.

4.1.2 Sub-Doppler TPE spectroscopy with the cw SPPC ECDL

A sub-Doppler TPE spectrum, recorded by tuning output (∼822.47 nm, 3 mW) from our cw SPPC ECDL system through the Cs $8s\ ^2S_{1/2} \leftarrow 6s\ ^2S_{1/2}$ ($F = 4$) two-photon hyperfine transition [98], is shown in Fig. 13. As explained above, the spectrum is acquired by photon counting the resulting $7P \rightarrow 6S$ fluorescence at ∼460 nm, with each data point integrated over 0.1 s after allowing the laser frequency to settle for 0.4 s. Incidentally, on a longer time-scale (>10 s), we have noticed a small, reproducible relaxation process associated with the setting of the PZT micropositioner.

A Lorentzian profile is found to fit the measured spectrum with a 3.1-MHz FWHM, to which there are several possible contributions in addition to the intrinsic optical bandwidth of the laser radiation itself [98–103]:

- The natural linewidth of ∼1 MHz.

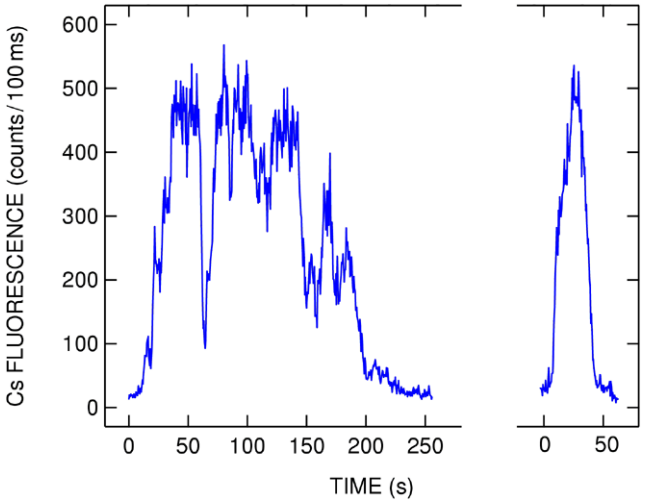

Fig. 14 Laser-frequency drift measured around the Cs $8s\ ^2S_{1/2} \leftarrow 6s\ ^2S_{1/2}$, $F = 4$ two-photon hyperfine transition at ∼822.4689 nm, as in Fig. 13. The *right-hand trace* shows that the free-running SPPC ECDL typically stays at the very narrow (∼3 MHz FWHM) resonance for ∼1 minute, or longer (see *left-hand trace*), implying a laser-frequency drift rate of ≤3 MHz min^{-1}

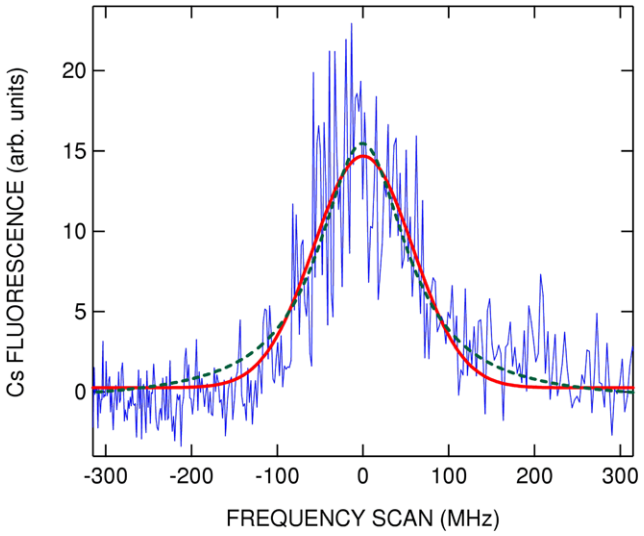

Fig. 15 Sub-Doppler TPE spectrum of the $8s\ ^2S_{1/2} \leftarrow 6s\ ^2S_{1/2}$, $F = 3$ hyperfine transition of atomic Cs, recorded (*fine trace*) by frequency-scanning coherent radiation at ∼822.4595 nm from the pulsed SAT OPO injection-seeded by the SPPC ECDL, fluorescence-detected in analog mode, both Gaussian (*solid trace*) and Lorentzian (*dashed trace*) fits to the shot-noise-limited observed feature have a 125-MHz FWHM. See text for further discussion

- A minor component of transit-time broadening associated with the beam waist (∼70-μm diameter) of the focused laser radiation.
- Pressure broadening, which has been measured [98] to be ∼0.75 MHz mTorr^{-1} and is therefore very small (<0.1 MHz) at our experimental sample pressure of ∼0.1 mTorr.

Two-photon spectral linewidths are known to be influenced by the nature of the laser noise [104], with a factor of two expected for Gaussian-type noise and a factor of four in the case of Lorentzian-type noise. On this basis, we estimate that the optical bandwidth of the laser radiation is ≤0.5 MHz FWHM. It is remarkable that this narrow optical bandwidth is attained in our SPPC ECDL system without active frequency stabilization or extensive mechanical, thermal, and acoustic isolation.

Operation of the SPPC ECDL system shows no sign of chaotic behavior and is insensitive to changes in diode current and temperature. From the typical time for the laser to stay at resonance with the sub-Doppler Cs two-photon transition, we infer that the drift rate of the laser frequency is less than ∼3 MHz min^{-1}. Two instances of such drift events (attributed to mechanical/thermal fluctuations) are portrayed in Fig. 14.

4.1.3 Sub-Doppler TPE spectroscopy with the pulsed SAT OPO

A second Cs $8s\ ^2S_{1/2} \leftarrow 6s\ ^2S_{1/2}$ sub-Doppler TPE spectrum (recorded at the same Cs sample pressure of ∼0.1 mTorr as in Fig. 13) is shown in Fig. 15. This is recorded by tuning signal output pulses (∼6 ns FWHM, non-Gaussian; ∼1 μJ per pulse) from our SAT OPO system through the $F = 3$ two-photon hyperfine transition at ∼822.46 nm [98] and using analog current-mode PMT detection of $7P \rightarrow 6S$ fluorescence at ∼460 nm. It is particularly noteworthy that this spectroscopic scan was performed without needing to make any mechanical or optoelectronic adjustment to the OPO cavity.

The quality of the spectrum in Fig. 15 is limited by the statistical shot-noise fluctuations that are inevitable, given the weakness of the fluorescence signal at a sample pressure as low as ∼0.1 mTorr. It is difficult to distinguish the adequacy of Gaussian (solid line) and Lorentzian (dashed line) fits to the pulsed TPE spectrum. Each fit yields a TPE linewidth of ∼125 MHz FWHM, which is to be compared with a predicted Fourier-transform-limited linewidth in the range of ∼70–150 MHz FWHM; the lower and upper limits correspond respectively to possible temporal-profile extremes of Gaussian and rectangular pulses, as discussed in our previous TPE spectroscopic studies of injection-seeded OPO bandwidths [96, 97].

In our preliminary report of the performance of the pulsed SAT OPO [9], we have explained that continuous, mode-hop-free SLM tunability of its signal output radiation is indicated by observing étalon interference fringes as the cw seed wavelength is slowly scanned. Additional spectroscopic demonstrations of the narrowband tunability of the pulsed SAT OPO are presented in Sect. 4.2 below.

4.2 Other pulsed OPO spectroscopic results

To demonstrate the pulsed SAT OPO's continuous narrowband tunability, we have previously reported [9] a high-resolution pulsed cavity-ringdown absorption spectrum of a single absorption feature of pure CO_2 gas (20 Torr, 300 K). This comprised a 4.5-GHz (0.15-cm^{-1}) scan over the 6948.762-cm^{-1} $P(24)$ line in the $3\nu_3$ band of CO_2, as registered in the HITRAN 2004 spectroscopic database [105], the spectrum was recorded by tuning the SAT OPO idler output at ∼1.439 μm, controlled by scanning the signal-wave wavelength (∼844.6 nm) of the seed laser. As in the context of Fig. 15, there was no need to make any mechanical or optoelectronic adjustment to the OPO cavity during such a spectroscopic scan. The data points (each averaged over 32 OPO pulses) are well fitted by a Lorentzian profile with a FWHM bandwidth of 507 MHz (0.017 cm^{-1}) was found to fit the CO_2 spectrum, consistent with a combination of Doppler and pressure broadening plus a minor contribution (≤100 MHz) from the optical bandwidth of the OPO idler radiation [9]. It is also possible that the spectrum was affected by minor fluctuations in the frequency of the Nd:YAG pump laser, which are transferred to the idler wave when the SAT OPO is injection-seeded at its signal wavelength. Note that such an uncertainty does not arise in the context of Fig. 15, where the frequency of the signal wave is determined by the SAT OPO cavity which is locked to the frequency of the injection seeder.

Another demonstration of the pulsed SAT OPO's spectroscopic efficacy is illustrated in Fig. 16. This comprises a pair of correlated cavity-ringdown absorption spectra recorded simultaneously by using the scanned complementary wavelengths of signal and idler outputs (∼822.3 and ∼1.508 μm, respectively) of the pulsed SAT OPO. The absorbing sample is H_2O vapor (25 Torr, 300 K) in a chamber containing two separate ringdown cavities, enabling portions of the $(2\nu_1+\nu_2+\nu_3)$ band at ∼12159.8 cm^{-1} and of the $(\nu_1+2\nu_2)$ band at ∼6629 cm^{-1} of H_2O to be recorded simultaneously as the respective signal- and idler-wave outputs of the SAT OPO are scanned. Unfortunately, the performance of our commercial 820–840-nm seed laser had deteriorated by the time these dual-wavelength spectra were recorded, so that relatively broad linewidths (∼0.25 cm^{-1} FWHM) are observed owing to multiple-longitudinal-mode operation of the seed source. Also plotted are stick spectra based on the HITRAN 2004 spectroscopic database [105]; the principal features are at 12159.811 cm^{-1} in the signal-wave spectrum and at 6628.256, 6628.910 and 6630.054 cm^{-1} in the idler-wave spectrum. In view of the energy-conservation condition of OPO operation, the two frequency scales sum to the frequency of the 532-nm pump source.

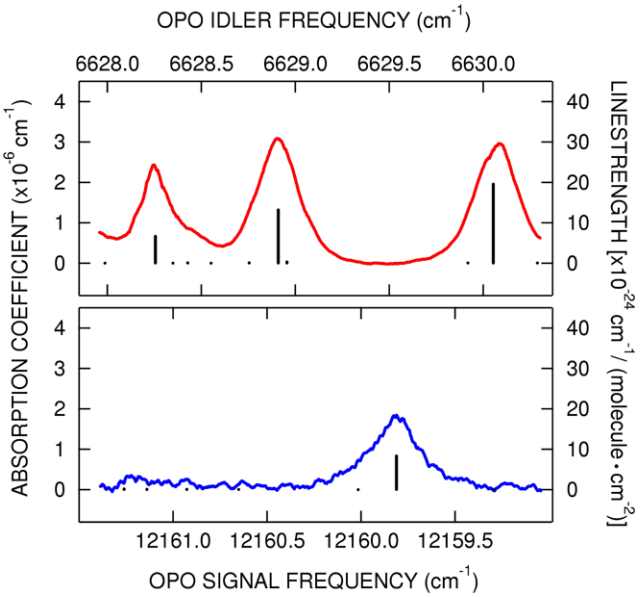

Fig. 16 Cavity-ringdown absorption spectra for portions of the $(2\nu_1+\nu_2+\nu_3)$ and $(\nu_1+2\nu_2)$ rovibrational bands of H_2O vapor (25 Torr, 300 K) at ∼12159.8 and ∼6629 cm^{-1}, recorded simultaneously by scanning the signal- and idler-output wavelengths of the pulsed injection-seeded SAT OPO, respectively. Stick spectra based on the HITRAN 2004 spectroscopic database are also plotted

5 Concluding discussion

In this paper, we have provided detailed information about the design and performance (notably SLM operation and continuous narrowband tunability) of two varieties of coherent near-infrared light source, namely:

(a) A pulsed, injection-seeded self-adaptive tunable (SAT) OPO [9], and
(b) A cw extended-cavity diode laser (ECDL) employing self-pumped PR feedback [10]

The realization of each of these devices (a) and (b), as described in Sects. 2 and 3 respectively, is facilitated by the photorefractivity of intracavity optical elements based on Rh:$BaTiO_3$ [8], in which dynamic phase-conjugate Bragg gratings are formed. Each of these is a clear manifestation of the use of photorefractivity to "reinforce the self-organizing process by an adaptive filter" [12] and thereby achieve SLM operation without any active mechanical adjustment. Applications of devices (a) and (b) to high-resolution spectroscopy have been indicated in Sect. 4, through assorted spectroscopic experiments (e.g., fluorescence-detected sub-Doppler two-photon absorption in Cs vapor [98–101]) that have been performed to verify the devices' performance.

In the former context (a), we note that the operation of our pulsed SAT OPO, with its *dynamically* prepared PR phase-conjugate Bragg grating and its narrowband SLM tuning capability, is in marked contrast to that of other OPO designs with a *static* PR Bragg grating. For instance, such

a PR grating, permanently written in PPLN by ultraviolet light, has been used for distributed-feedback operation of a pulsed PPLN OPO [48] at fixed signal and idler wavelengths of 1.439 and 4.085 μm, respectively, when the PPLN OPO is pumped at 1.064 μm or at 619.3 nm and 3.774 μm when it is pumped at 532 nm; however, this is a less dynamic and adaptable arrangement than in our SAT OPO [9] and the optical bandwidth of ∼0.3 nm (∼1.5 cm^{-1}) from the DFB OPO is inferior to the optical bandwidth of ≤150 MHz (≤0.005 cm^{-1}) that we infer from Fig. 15. Likewise, tunable ns-pulsed OPOs that incorporate a volume Bragg grating (VBG) retro-reflector have been reported [106–109]. One of these VBG OPOs [107] is based on 1.064-μm-pumped MgO-doped PPLN, has signal- and idler-tuning ranges of 1.97–2.04 μm and 2.31–2.22 μm, respectively, with a maximum output pulse energy of 61 mJ and 44% slope efficiency at the degeneracy point (2.128 μm). Another is a compact tunable 532-nm-pumped PPKTP OPO [108, 109] that delivers signal output at ∼760 nm with a VBG-facilitated tuning range of ∼2.6 THz (∼87 cm^{-1}) and ∼130-GHz (∼4.3-cm^{-1}) optical bandwidth. We also note in this context that the long-anticipated [110] but only recently demonstrated [111] backward (mirrorless) OPO has been likened [112] to the nonlinear-optical equivalent of a DFB laser, which does not require any conventional mirrors (compared to our one-mirror SAT OPO design [9]).

The design of our SAT OPO (a) is robust and simple, providing a remarkably straightforward way to achieve reliable narrowband (SLM) tuning of OPO signal and idler output, without any need for active mechanical or optoelectronic adjustment of the OPO cavity. To achieve this, we have taken advantage of the high photorefractive efficiency of Rh:$BaTiO_3$ which can be used with seed radiation (e.g., from an independently tunable narrowband ECDL) at near-infrared wavelengths (0.6–1.1 μm). Other photorefractive materials may be suitable for SAT OPOs that are injection-seeded at longer infrared wavelengths, such as the particularly topical 1.55-μm optical telecommunications band. For example, the semi-conducting material vanadium-doped cadmium telluride (V:CdTe) [113] has been used as an adaptive intracavity filter to facilitate SLM tuning of an ECDL operating at ∼1.55 μm [26]. Another inorganic PR material that may be of interest in this context is tin hypothiodiphosphate ($Sn_2P_2S_6$) [114–118]; for instance, tellurium-doping of $Sn_2P_2S_6$ enables high-speed photorefraction at ∼1.55 μm [117].

In the context of our SPPC ECDL design (b), with its self-pumped PR feedback and intracavity compact high-finesse intracavity ring filter [10], we have demonstrated a new scheme for passive frequency stabilization and SLM tuning that is robust and well-controlled. This scheme has been characterized by using a Fabry–Perot laser diode operating around 820–840 nm and its high performance verified via sub-Doppler TPE spectra of $8S \leftarrow 6S$ transitions in Cs atoms. Our SPPC ECDL design (b) joins many other approaches to PR phase-conjugate feedback control of ECDLs [10, 12, 14, 20–43]; it results in a low-drift narrowband SLM-tunable laser source that provides a relatively economical way to refine the spectroscopic utility of a simple Fabry–Perot diode laser. We expect that it will be useful for high-resolution measurements, in particular for atomic laser spectroscopy and as an injection seeder for narrowband pulsed nonlinear-optical coherent light sources applied to high-precision spectroscopy [9, 58–65].

Acknowledgements We appreciate the valuable research contributions of John Carew and Richard White to early phases of this project. We acknowledge financial support from the Australian Research Council.

References

1. P. Günter, J.-P. Huignard (eds.), *Photorefractive Materials and Their Applications I*. Topics in Applied Physics, vol. 61 (Springer, Berlin, 1988)
2. P. Günter, J.-P. Huignard (eds.), *Photorefractive Materials and Their Applications II*. Topics in Applied Physics, vol. 62 (Springer, Berlin, 1988)
3. P. Yeh, *Introduction to Photorefractive Nonlinear Optics* (Wiley, New York, 1993)
4. F.M. Davidson (ed.), *Selected Papers on Photorefractive Materials*. SPIE Milestone Series, vol. MS 86 (The Society of Photo-Optical Instrumentation Engineers, Bellingham, 1994)
5. P. Günter, J.-P. Huignard (eds.), *Photorefractive Materials and Their Applications 1—Basic Effects*. Springer Series in Optical Physics, vol. 113 (Springer, New York, 2006)
6. P. Günter, J.-P. Huignard (eds.), *Photorefractive Materials and Their Applications 2—Materials*. Springer Series in Optical Physics, vol. 114 (Springer, New York, 2006)
7. P. Günter, J.-P. Huignard (eds.), *Photorefractive Materials and Their Applications 3—Applications*. Springer Series in Optical Physics, vol. 115 (Springer, New York, 2006)
8. M.B. Klein, Photorefractive properties of $BaTiO_3$, in *Photorefractive Materials and Their Applications 2—Materials*, ed. by P. Günter, J.-P. Huignard. Springer Series in Optical Physics, vol. 114 (Springer, New York, 2006), pp. 241–284, Chap. 8
9. Y. He, B.J. Orr, Opt. Lett. **29**, 2169 (2004)
10. Y. He, B.J. Orr, Opt. Lett. **33**, 2368 (2008)
11. B. Fischer, S. Sternklar, S. Weiss, IEEE J. Quantum Electron. **25**, 550 (1989)
12. G. Pauliat, N. Dubreuil, G. Roosen, Self-organizing laser cavities, in *Photorefractive Materials and Their Applications 3—Applications*, ed. by P. Günter, J.-P. Huignard. Springer Series in Optical Physics, vol. 115 (Springer, New York, 2007), pp. 253–275, Chap. 9
13. L. Lombard, A. Brignon, J.-P. Huignard, E. Lallier, P. Georges, G. Lucas-Leclin, G. Pauliat, G. Roosen, C.R., Phys. **8**, 234 (2007)
14. T. Omatsu, M.J. Damzen, A. Minassian, K. Kuroda, Solid-state lasers with a photorefractive phase-conjugate mirror, in *Photorefractive Materials and Their Applications 3—Applications*, ed. by P. Günter, J.-P. Huignard. Springer Series in Optical Physics, vol. 115 (Springer, New York, 2007), pp. 193–221, Chap. 7
15. N. Huot, J.M. Jonathan, G. Pauliat, P. Georges, A. Brun, G. Roosen, Appl. Phys. B **69**, 155 (1999)

16. T. Omatsu, M.J. Damzen, Opt. Commun. **198**, 135 (2001)
17. B.K. Das, H. Suche, W. Sohler, Appl. Phys. B **73**, 439 (2001)
18. T. Omatsu, A. Minassian, M.J. Damzen, Jpn. J. Appl. Phys., Part 1 **41**(4A), 2024 (2002)
19. B.K. Das, R. Ricken, V. Quiring, H. Suche, W. Sohler, Opt. Lett. **29**, 165 (2004)
20. M. Cronin-Golomb, A. Yariv, Opt. Lett. **11**, 455 (1986)
21. K. Vahala, K. Kyuma, A. Yariv, S.K. Kwong, M. Cronin-Golomb, K.Y. Lau, Appl. Phys. Lett. **49**, 1563 (1986)
22. B.W. Liby, D. Statman, IEEE J. Quantum Electron. **32**, 835 (1996)
23. A. Shiratori, M. Obara, Appl. Phys. Lett. **69**, 1515 (1996)
24. A. Shiratori, M. Obara, Appl. Phys. B **65**, 329 (1997)
25. J.S. Lawrence, D.M. Kane, Phys. Rev. A **63**, 033805 (2001)
26. A. Godard, G. Pauliat, G. Roosen, P. Graindorge, P. Martin, Opt. Lett. **26**, 1955 (2001)
27. S. Maerten, N. Dubreuil, G. Pauliat, G. Roosen, D. Rytz, T. Salva, Opt. Commun. **208**, 183 (2002)
28. A. Godard, G. Pauliat, G. Roosen, E. Ducloux, Appl. Opt. **43**, 3543 (2004)
29. C. Pedersen, R.S. Hansen, Opt. Express **13**, 3961 (2005)
30. M. Vainio, IEEE Photonics Technol. Lett. **18**, 2047 (2006)
31. M. Segev, Y. Ophir, B. Fischer, G. Eisenstein, Appl. Phys. Lett. **57**, 2523 (1990)
32. S. MacCormack, J. Feinberg, M.H. Garrett, Opt. Lett. **19**, 120 (1994)
33. T. Omatsu, A. Katoh, K. Okada, S. Hatano, A. Hasegawa, M. Tateda, I. Ogura, Opt. Commun. **146**, 167 (1998)
34. M. Løbel, P.M. Petersen, P.M. Johansen, Appl. Phys. Lett. **72**, 1263 (1998)
35. M. Løbel, P.M. Petersen, P.M. Johansen, J. Opt. Soc. Am. B **15**, 2000 (1998)
36. M. Løbel, P.M. Petersen, P.M. Johansen, Opt. Lett. **23**, 825 (1998)
37. H. Horiuchi, T. Shimura, T. Omatsu, O. Matoba, K. Kuroda, Appl. Phys. B **68**, 1021 (1999)
38. J.S. Lawrence, D.M. Kane, J. Lightw. Technol. **20**, 100 (2002)
39. P.D. van Voorst, H.L. Offerhaus, K.-J. Boller, Opt. Lett. **31**, 1061 (2006)
40. V. Reboud, N. Dubreuil, P. Fournet, G. Pauliat, G. Roosen, D. Rytz, Opt. Express **14**, 2735 (2006)
41. V. Reboud, N. Dubreuil, P. Fournet, G. Pauliat, G. Roosen, D. Rytz, Appl. Phys. B **87**, 233 (2007)
42. P.D. van Voorst, M.R. de Wit, H.L. Offerhaus, S. Tay, J. Thomas, N. Peyghambarian, K.-J. Boller, Opt. Express **15**, 17587 (2007)
43. B. Terhalle, N. Radwell, P. Rose, C. Denz, T. Ackemann, Appl. Phys. Lett. **93**, 151114 (2008)
44. W.B. Whitten, J.M. Ramsey, Opt. Lett. **9**, 44 (1984)
45. J. Feinberg, G.D. Bacher, Opt. Lett. **9**, 420 (1984)
46. M. Bode, I. Freitag, A. Tunnermann, H. Welling, P.K. Lam, H.-A. Bachor, High power operation of a continuously-tunable doubly resonant optical parametric oscillator, in *OSA Trends in Optics and Photonics*. Advanced Solid State Lasers, vol. 19 (Opt. Soc. Am., Washington, 1998), pp. 136–141
47. S. Victori, T. Lepine, P. Georges, A. Brun, Spectral narrowing of a pulsed optical parametric oscillator using an intracavity photorefractive crystal, in *OSA Trends in Optics and Photonics*. Advanced Solid-State Lasers, vol. 68 (Opt. Soc. Am., Washington, 2002), pp. 66–69
48. A.C. Chiang, Y.Y. Lin, T.D. Wang, Y.C. Huang, J.T. Shy, Opt. Lett. **27**, 1815 (2002)
49. S.E. Harris, Proc. IEEE **57**, 2096 (1969)
50. R.L. Byer, Parametric oscillators, in *Laser Spectroscopy*, ed. by R.G. Brewer, A. Mooradian (Plenum, New York, 1973), pp. 77–101
51. R.L. Byer, Optical parametric oscillators, in *Quantum Electronics: A Treatise, vol. I, Nonlinear Optics, Part B*, ed. by H. Rabin, C.L. Tang (Academic Press, New York, 1975), pp. 587–702, Chap. 9
52. R.L. Byer, R.L. Herbst, Parametric oscillation and mixing, in *Nonlinear Infrared Generation*, ed. by Y.-R. Shen (Springer, Berlin, 1977), pp. 81–137, Chap. 3
53. S.J. Brosnan, R.L. Byer, IEEE J. Quantum Electron. **QE-15**, 415 (1979)
54. B.J. Orr, M.J. Johnson, J.G. Haub, Spectroscopic applications of pulsed tunable optical parametric oscillators, in *Tunable Laser Applications*, 1st edn., ed. by F.J. Duarte (Dekker, New York, 1995), pp. 11–82, Chap. 2
55. I.T. Sorokina, K.L. Vodopyanov (eds.), *Solid-State Mid-Infrared Sources* (Springer, Berlin, 2003)
56. M. Ebrahim-Zadeh, I.T. Sorokina (eds.), *Mid-Infrared Coherent Sources and Applications*. NATO Science for Peace and Security Series B: Physics and Biophysics (Springer, Berlin, 2007)
57. B.J. Orr, Y. He, R.T. White, Spectroscopic applications of tunable optical parametric oscillators, in *Tunable Laser Applications*, 2nd edn., ed. by F.J. Duarte (CRC Press, New York, 2009), pp. 15–95, Chap. 2
58. G.W. Baxter, H.-D. Barth, B.J. Orr, Appl. Phys. B **66**, 653 (1998)
59. G.W. Baxter, Y. He, B.J. Orr, Appl. Phys. B **67**, 753 (1998)
60. Y. He, G.W. Baxter, B.J. Orr, Rev. Sci. Instrum. **70**, 3203 (1999)
61. G.W. Baxter, M.A. Payne, B.D.W. Austin, C.A. Halloway, J.G. Haub, Y. He, A.P. Milce, J.W. Nibler, B.J. Orr, Appl. Phys. B **71**, 651 (2000)
62. Y. He, B.J. Orr, Appl. Opt. **40**, 4836 (2001)
63. R.T. White, Y. He, B.J. Orr, M. Kono, K.G.H. Baldwin, Opt. Lett. **28**, 1248 (2003)
64. R.T. White, Y. He, B.J. Orr, M. Kono, K.G.H. Baldwin, J. Opt. Soc. Am. B **21**, 1586 (2004)
65. R.T. White, Y. He, B.J. Orr, M. Kono, K.G.H. Baldwin, J. Opt. Soc. Am. B **24**, 2601 (2007)
66. O.J. Votava, R. Fair, D.F. Plusquellic, E. Riedle, D.J. Nesbitt, J. Chem. Phys. **107**, 8854 (1997)
67. M.J.T. Milton, T.D. Gardiner, F. Molero, J. Galech, Opt. Commun. **142**, 153 (1997)
68. A. Borsutzky, Quantum Semiclass. Opt. **9**, 191 (1997)
69. A. Fix, V. Weiss, G. Ehret, Pure Appl. Opt. **7**, 837 (1998)
70. S. Wu, V.A. Kapinus, G.A. Blake, Opt. Commun. **159**, 74 (1999)
71. J.A.J. Fitzpatrick, O.V. Chekhlov, J.M.F. Elks, C.M. Western, S.H. Ashworth, J. Chem. Phys. **115**, 6920 (2001)
72. W.D. Kulatilaka, T.N. Anderson, T.L. Bougher, R.P. Lucht, Appl. Phys. B **80**, 669 (2005)
73. P. Mahnke, H.H. Klingenberg, A. Fix, M. Wirth, Appl. Phys. B **89**, 1 (2007)
74. K.O. Hill, G. Meltz, J. Lightw. Tech. **15**, 1263 (1997)
75. V.G. Dmitriev, G.G. Gurzayan, D.N. Nikogosyan, *Handbook of Nonlinear Optical Crystals*, 3rd edn. (Springer, New York, 1999)
76. A.V. Smith, SNLO nonlinear optics code. Public domain software downloadable from www.as-photonics.com/?q=SNLO, Version 43. Accessed November 28, 2008
77. H. Stoehr, F. Mensing, J. Helmcke, U. Sterr, Opt. Lett. **31**, 736 (2006)
78. B. Dahmani, L. Hollberg, R. Drullinger, Opt. Lett. **12**, 876 (1987)
79. D.A. King, R.J. Pittaro, Opt. Lett. **23**, 774 (1998)
80. R. Ludeke, E.P. Harris, Appl. Phys. Lett. **20**, 499 (1972)
81. R. Wyatt, W.J. Devlin, Electron. Lett. **19**, 110 (1983)
82. M.R. Matthews, K.H. Cameron, R. Wyatt, W.J. Devlin, Electron. Lett. **21**, 113 (1985)
83. C.E. Wieman, L. Hollberg, Rev. Sci. Instrum. **62**, 1 (1991)
84. K.C. Harvey, C.J. Myatt, Opt. Lett. **16**, 910 (1991)
85. F. Favre, D. Le Guen, Electron. Lett. **27**, 183 (1991)

86. M. de Labachelerie, P. Cerez, Opt. Commun. **55**, 174 (1994)
87. P. Zorabedian, IEEE J. Quantum Electron. **30**, 1542 (1994)
88. P. Zorabedian, Tunable external-cavity semiconductor lasers, in *Tunable Lasers Handbook*, ed. by F.J. Duarte (Academic Press, San Diego, 1995), pp. 349–442, Chap. 8
89. A. Godard, G. Pauliat, G. Roosen, P. Graindorge, P. Martin, IEEE J. Quantum Electron. **38**, 390 (2002)
90. M. Løbel, J. Appl. Phys. **84**, 3483 (1998)
91. R.S. Putnam, D.G. Lancaster, Appl. Opt. **38**, 1513 (1999)
92. J.M. Boon-Engering, W.E. van der Veer, J.W. Gerritsen, W. Hogervorst, Opt. Lett. **20**, 380 (1995)
93. M.J. Johnson, J.G. Haub, B.J. Orr, Opt. Lett. **20**, 1277 (1995)
94. J.G. Haub, R.M. Hentschel, M.J. Johnson, B.J. Orr, J. Opt. Soc. Am. B **12**, 2128 (1995)
95. W.D. Kulatilaka, T.N. Anderson, T.L. Bougher, R.P. Lucht, Appl. Phys. B **80**, 669 (2005)
96. M. Kono, K.G.H. Baldwin, Y. He, R.T. White, B.J. Orr, Opt. Lett. **30**, 3413 (2005)
97. M. Kono, K.G.H. Baldwin, Y. He, R.T. White, B.J. Orr, J. Opt. Soc. Am. B **23**, 1181 (2006)
98. C. Hagel, C. Nesi, L. Jozefowski, C. Schwob, F. Nez, F. Biraben, Opt. Commun. **160**, 1 (1999)
99. J. Marek, Phys. Lett. A **60**, 190 (1977) and references therein
100. P. Fendel, D. Bergeson, T. Udem, T.W. Hänsch, Opt. Lett. **32**, 701 (2007)
101. K. Sasaki, K. Sugiyama, V. Babychev, A. Onae, Jpn. J. Appl. Phys., Part 1 **39**(9A), 5310 (2000)
102. C.-Y. Cheng, C.-M. Wu, G.B. Liao, W.-Y. Cheng, Opt. Lett. **32**, 563 (2007)
103. W.-Y. Cheng, T.-H. Wu, S.-W. Huang, S.-Y. Lin, C.-M. Wu, Appl. Phys. B **92**, 13 (2008)
104. D.S. Elliott, M.W. Hamilton, K. Arnett, S.J. Smith, Phys. Rev. A **32**, 887 (1985)
105. L.S. Rothman, D. Jacquemart, A. Barbe, D.C. Benner, M. Birk, L.R. Brown, M.R. Carleer, C. Chackerian Jr., K. Chance, L.H. Coudert, V. Dana, V.M. Devi, J.-M. Flaud, R.R. Gamache, A. Goldman, J.-M. Hartmann, K.W. Jucks, A.G. Maki, J.-Y. Mandin, S.T. Massie, J. Orphal, A. Perrin, C.P. Rinsland, M.A.H. Smith, J. Tennyson, R.N. Tolchenov, R.A. Toth, J. Vander Auwera, P. Varanasi, G. Wagner, J. Quantum Spectrosc. Radiat. Transf. **96**, 139 (2005)
106. B. Jacobsson, M. Tiihonen, V. Pasiškevičius, F. Laurell, Opt. Lett. **30**, 2281 (2005)
107. J. Saikawa, M. Fujii, H. Ishizuki, T. Taira, Opt. Lett. **32**, 2996 (2007)
108. B. Jacobsson, C. Canalias, V. Pasiškevičius, F. Laurell, Opt. Lett. **32**, 3278 (2007)
109. J.E. Hellström, B. Jacobsson, V. Pasiškevičius, F. Laurell, IEEE J. Quantum Electron. **44**, 81 (2008)
110. S.E. Harris, Appl. Phys. Lett. **9**, 114 (1966)
111. C. Canalias, V. Pasiškevičius, Nat. Photonics **1**, 459 (2007)
112. J.B. Khurgin, Nat. Photonics **1**, 446 (2007)
113. A. Partovi, J. Millerd, E.M. Garmire, M. Ziari, W.H. Steier, S.B. Trivedi, M.B. Klein, Appl. Phys. Lett. **57**, 846 (1990)
114. M. Jazbinšek, G. Montemezzani, P. Günter, A.A. Grabar, I.M. Stoika, Y.M. Vysochanskii, J. Opt. Soc. Am. B **24**, 1241 (2003)
115. A.A. Grabar, M. Jazbinšek, A.N. Shumelyuk, Y.M. Vysochanskii, G. Montemezzani, P. Günter, Photorefractive effects in $Sn_2P_2S_6$, in *Photorefractive Materials and Their Applications 2—Materials*, ed. by P. Günter, J.-P. Huignard. Springer Series in Optical Physics, vol. 114 (Springer, New York, 2007), pp. 327–362, Chap. 10
116. T. Bach, M. Jazbinšek, G. Montemezzani, P. Günter, A.A. Grabar, Y.M. Vysochanskii, J. Opt. Soc. Am. B **24**, 1535 (2007)
117. R. Mosimann, P. Marty, T. Bach, F. Juvalta, M. Jazbinšek, P. Günter, A.A. Grabar, Opt. Lett. **32**, 3230 (2007)
118. F. Juvalta, R. Mosimann, M. Jazbinšek, P. Günter, Opt. Express **17**, 379 (2009)